Spatiotemporal Patterns Induced by Turing-Hopf Interaction and Symmetry on a Disk

Yaqi Chen

Department of Mathematics, Harbin Institute of Technology,

Weihai, Shandong 264209, People's Republic of China

Xianyi Zeng

Department of Mathematics, Lehigh University,

Bethlehem, Pennsylvania 18015, USA

Ben Niu *

Department of Mathematics, Harbin Institute of Technology,

Weihai, Shandong 264209, People's Republic of China

(*Corresponding author: niu@hit.edu.cn)

Abstract

Turing bifurcation and Hopf bifurcation are two important kinds of transitions giving birth to inhomogeneous solutions, in spatial or temporal ways. On a disk, these two bifurcations may lead to equivariant Turing-Hopf bifurcations, whose normal forms are given in three different cases in this paper. In addition, we analyzed the possible solutions for each normal form, which can guide us to find solutions with physical significance in real-world systems, and the breathing, standing wave-like, and rotating wave-like patterns are found in a delayed mussel-algae model.

I. INTRODUCTION

Complex spatiotemporal patterns that appear on approximate circular domains are abundant and absorbing, such as the distribution of microbial bioherms in irregular natural or artificial lakes [1, 2], spiral waves generated by the interaction of activator and inhibitor in Petri dishes [3, 4], and rotating waves in an optical system consisting of a thin Kerr nonlinear layer and a feedback loop [5, 6], and so on. To comprehend and manage these dynamic phenomena effectively, modeling with reaction-diffusion equations and analysis through Turing-Hopf bifurcations are proved to be essential tools. Such approaches offer valuable insights into the future management of some fragile ecosystems [7, 8], the formation mechanisms of spiral waves in fibrous ventricular fibrillation and tachycardia [9, 10], and enable pattern selection and control, thereby expanding the scope of optical information processing [11, 12]. Mathematically, in the case of planar waves, the solution to the reaction-diffusion equation is given by $u_j(\vec{x},t) = u_{j_0} e^{i\vec{q}\cdot\vec{x}+\sigma t}$ [13], where $\vec{q}$ is the wave vector and σ is the eigenvalue with the largest real part. For a point where both Turing instability [14] and Hopf bifurcation [15–17] occur, or Turing-Hopf bifurcation point we say, $\vec{q}$ is nonzero and σ is also an imaginary value $i\omega$. Thus, there exists the interaction of two Fourier modes, which is accompanied by quite complicated dynamics [18–21]. The wave solutions on circular domains mentioned above are also important, and we will study them in this paper.

Turing-Hopf bifurcation has been studied both numerically and analytically in the literature [22–28]. In recent years, scholars have begun to use normal forms to analyze Turing-Hopf bifurcation. In particular, Song et al. [29] and Jiang et al. [30] extended the results in Ref. [31] and derived the normal form of the Turing-Hopf bifurcation of partial differential equations (PDEs) and partial functional differential equations (PFDEs), respectively. Following the method proposed, there are many subsequent works on normal forms of the Turing-Hopf bifurcation [32–37]. The recently developed analytical tool using normal form is adopted in the current work.

However, most of these works have focused on one-dimensional intervals and cannot better describe the complex patterns that occur in high-dimensional domains. In fact, the complex spatiotemporal patterns appearing in circular domains can be studied through equivariant bifurcation [38, 39]. That is to say, the existence of symmetry leads to the multiplicity of eigenvalues, and some more complex phenomena may occur under the influence of symmetric groups. In previous works, inspired by theories of the symmetric group [38] and equivariant normal forms [39–41], we provided approximate expressions for periodic solutions generated by the Hopf bifurcation,

including the rotating wave and the standing wave solution on a circular domain in [42]. Equivariant Turing-Hopf bifurcation on a disk has not been considered, to our best knowledge. Therefore, in this paper, we shall consider a general reaction-diffusion system with homogeneous Neumann boundary conditions on a disk and aim to explain more complicated spatiotemporal patterns induced by Turing-Hopf interaction and symmetry.

Compared to previous work, this paper has several additional features. We derive formulas of the equivariant normal forms truncated to the third order of a general reaction-diffusion system on a disk and divide them into three types: *ET-H*, *T-EH*, and *ET-EH bifurcations*, according to the different structure of the center subspace of the equilibrium. We characterize the long-term asymptotic behavior of the solution by normal forms, which can explain the occurrence of many patterns in real life more fitly. The theoretical results indicate the existence of several kinds of interesting patterns, several of which are unique to the equivariant Turing-Hopf bifurcation, including *mixed ET-EH*, *breathing*, *quasi-periodic ET-H*, *standing wave-like T-EH*, *rotating wave-like patterns T-EH* patterns.

The rest of the paper is organized as follows. In Sec. II, we provide preliminaries required for normal form derivation, including the introduction to the model, the definition of phase space, the eigenvalue problem of the Laplace operator on a circular domain, and the necessary assumptions for bifurcations. In Sec. III, we prove the main results of normal forms for *ET-H*, *T-EH*, and *ET-EH bifurcations* on a disk, respectively, and provide the classification of various pattern solutions. In Sec. IV, to verify the theory, we study two delayed mussel-algae systems numerically. Rich spatiotemporal patterns are observed near the Turing-Hopf points.

II. ANALYTICAL PRELIMINARIES

This section begins with an explanation of the reaction-diffusion equation studied and we provide some simple results on characteristic equations and sufficient conditions for the existence of bifurcations through traditional linearization methods.

A. Mathematical model

The reaction-diffusion equation stands as an important theoretical model in the fields of ecology, medicine, chemistry, physics, and so on, which provides valuable insights into the understand-

ing of interesting phenomena that occur in complex systems. Its general formulation is

$$\frac{\partial u}{\partial t} = d\Delta u + f(u),$$

where Δ denotes the Laplacian, d represents the diffusion coefficient and f is the kinetic function. In many scenarios, it is necessary to establish a reaction-diffusion system, incorporating multiple equations to characterize distinct interaction processes through the varied selection of f. Examples include predator-prey behavior [43–46], disease infection [47, 48], chemical reactions [49, 50], semiconductor charge transport in heterostructure devices [23, 25], and so on. Additionally, considering factors such as biological maturation periods, the time required for energy conversion in biological systems or chemical reactions, incubation periods, and charge transfer times, introducing time delay in reaction-diffusion systems can better depict real-world situations.

Taking these factors into consideration, we select a general delayed reaction-diffusion system of n equations with *homogeneous Neumann boundary conditions* defined on a disk as follows:

$$\frac{\partial U(t,r,\theta)}{\partial t} = D(\nu)\Delta_{r\theta}U(t,r,\theta) + L(\nu)U_t(r,\theta) + F\left(U_t(r,\theta),\nu\right),\ (r,\theta)\in\mathbb{D},\ t>0, \qquad (1)$$

where $D(\nu) = \mathrm{diag}\{d_1(\nu), d_2(\nu), \cdots, d_n(\nu)\}$, $\Delta_{r\theta} = \frac{\partial^2}{\partial r^2} + \frac{1}{r}\cdot\frac{\partial}{\partial r} + \frac{1}{r^2}\cdot\frac{\partial^2}{\partial\theta^2}$ represents the Laplace operator on a disk $\mathbb{D} = \{(r,\theta) : 0 \le r \le R, 0 \le \theta \le 2\pi\}$, ν represents the sum of the system control parameters, $L(\nu)$ is a linear operator that preserves the eigenspace of the Laplace operator, and $F(\nu)$ can be genuine nonlinear. $U_t(\vartheta)(r,\theta) = U(t+\vartheta,r,\theta),\ \vartheta\in[-1,0)$. Here, we normalize the maximum delay to 1, so that the time delay τ can be included in the parameter ν. The parameters in the kinetic functions have a certain possibility of inducing Hopf bifurcations, among which the time delay τ is most commonly selected as the bifurcation parameter. In addition, the diffusion coefficient is often used as an important parameter to induce Turing instability. When studying the interaction between Turing instability and Hopf bifurcation, which is generally of codimension-two, we set $\nu = (\nu_1,\nu_2)\in\mathbb{R}^2$. This is a general representation, which means that any two parameters in the equation can be chosen as the bifurcation parameters of inducing Turing-Hopf bifurcations. For example, if we focus on the impact of the diffusion coefficient in the first equation and the time delay on bifurcation phenomenon, we can choose $\nu = (d_1,\tau)$, and other diffusion parameters are fixed as constants.

When considering a reaction-diffusion equation with time delay, one usually use the phase space of functions $\mathscr{C} := C([-1,0],\mathscr{X}_{\mathbb{C}})$ [51, 52], where $\mathscr{X}_{\mathbb{C}}$ is the complexification of $\mathscr{X} =$

$\left\{\tilde{u}(r,\theta)\in W^{2,2}(\mathbb{D}):\partial_r\tilde{u}(R,\theta)=0,\ \theta\in[0,2\pi)\right\}$, with $\mathbb{L}^2$ inner product (weighted r)

$$\langle u(r,\theta),v(r,\theta)\rangle=\iint_{\mathbb{D}} ru(r,\theta)\bar{v}(r,\theta)\mathrm{d}r\mathrm{d}\theta.$$

Then, $U_t\in\mathscr{C}^n$, $L:\mathbb{R}\times\mathscr{C}^n\to\mathscr{X}_{\mathbb{C}}^n$ is a bounded linear operator, and $F:\mathscr{C}^n\times\mathbb{R}\to\mathscr{X}_{\mathbb{C}}^n$, where n is the number of equations included in the reaction-diffusion system (1). Here we only consider the zero equilibrium, that is to say, we assume $F(0,\nu)=0$, $D_\varphi F(0,\nu)=0$ that stands for the Fréchet derivative of $F(\varphi,\nu)$ with respect to φ at $\varphi=0$, $\forall\nu\in\mathbb{R}^2$, and F is C^k $(k\geq 3)$.

B. Linearization analysis

Linearising (1) around the zero equilibrium gives

$$\frac{\partial U(t,r,\theta)}{\partial t}=D(\nu)\Delta_{r\theta}U(t,r,\theta)+L(\nu)U_t(r,\theta). \tag{2}$$

The characteristic equation of the linearized equation (2) is

$$\prod_p\Gamma_p(\gamma)\prod_{n,m}\Gamma_{nm}(\gamma)=0, \tag{3}$$

with

$$\Gamma_p(\gamma)=\det\left[\gamma I+\lambda_p D(\nu)-L(\nu)(\mathrm{e}^{\gamma\cdot}I)\right]=0,\ p=0,1,2,\cdots,$$
$$\Gamma_{nm}(\gamma)=\det\left[\gamma I+\lambda_{nm}D(\nu)-L(\nu)(\mathrm{e}^{\gamma\cdot}I)\right]^2=0,\ n=1,2,\cdots,\ m=1,2,\cdots,$$

and

$$\lambda=\begin{cases}\lambda_p=\frac{\alpha_p^2}{R^2}, & p=0,1,2,\cdots,\\ \lambda_{nm}=\frac{\alpha_{nm}^2}{R^2},\ n=1,2,\cdots,\ m=1,2,\cdots,\end{cases}$$

where $-\alpha_p$ and $-\alpha_{nm}$ are eigenvalues of the Laplacian on the unit disk, see [42, 53] and the corresponding normalized eigenfuncitons are expressed from Bessel functions J_0,J_n by

$$\hat{\phi}=\begin{cases}\hat{\phi}_p^c, & p=0,1,2,\cdots,\\ \hat{\phi}_{nm}^c,\ \phi_{nm}^s,\ n=1,2,\cdots,\ m=1,2,\cdots,\end{cases}$$

with

$$\hat{\phi}_p^c=\frac{J_0\left(\frac{\alpha_p}{R}r\right)}{\|J_0\left(\frac{\alpha_p}{R}r\right)\|},\ \hat{\phi}_{nm}^c=\frac{J_n\left(\frac{\alpha_{nm}}{R}r\right)\mathrm{e}^{\mathrm{i}n\theta}}{2\pi\|J_n\left(\frac{\alpha_{nm}}{R}r\right)\|},\ \hat{\phi}_{nm}^s=\overline{\hat{\phi}_{nm}^c}=\frac{J_n\left(\frac{\alpha_{nm}}{R}r\right)\mathrm{e}^{-\mathrm{i}n\theta}}{2\pi\|J_n\left(\frac{\alpha_{nm}}{R}r\right)\|},$$

which form an orthonormal basis for $\mathscr{X}_{\mathbb{C}}$.

To consider the interaction of Turing instability and Hopf bifurcation, assuming that there exists a vector $\nu^*=(\nu_1^*,\nu_2^*)\in\mathbb{R}^2$, such that one of the situations in Table I holds. Inspired by [38, 39],

TABLE I: Roots with zero real part of (3) and the dimension of the central subspace (dim).

	(ET-H)	(T-EH)	(ET-EH)
$\Gamma_p = 0$	$\pm \mathrm{i}\omega_{H_1}$	0	———
$\Gamma_{nm} = 0$	0 (repeated)	$\pm \mathrm{i}\omega_{H_2}$ (repeated)	0 (repeated), $\pm \mathrm{i}\omega_{H_3}$ (repeated)
p,n,m	$p = p_{H_1}, n = n_{T_1}, m = m_{T_1}$	$p = p_{T_2}, n = n_{H_2}, m = m_{H_2}$	$n = n_{T_3}, m = m_{T_3}, n = n_{H_3}, m = m_{H_3}$ [a]
dim	4	5	6

[a] In (ET-EH), for example, the chosen indexes mean that $\Gamma_{n_{T_3} m_{T_3}}(0) = 0,\ \Gamma_{n_{H_3} m_{H_3}}(\pm \mathrm{i}\omega_{H_3}) = 0$.

if (ET-H) holds, we call this is a *ET-H bifurcation*, which means, the center space is spanned by the eigenvectors of a repeated semi-simple zero eigenvalue (multiplicity 2) and a pair of simple imaginary roots. Similarly, if (T-EH) holds, we call this a *T-EH bifurcation*. If (ET-EH) holds, we call this a *ET-EH bifurcation*.

To study the spatiotemporal dynamic behavior near the critical point $\nu = \nu^*$, it is necessary to introduce a new perturbation parameter $\mu = (\mu_1, \mu_2) = (\nu_1 - \nu_1^*, \nu_1 - \nu_2^*) = \nu - \nu^*$. Then, system (1) is equivalent to

$$\frac{\partial U(t)}{\partial t} = \tilde{L}(\mu) U_t + \tilde{F}(U_t, \mu), \tag{4}$$

where $\tilde{L}U = D_0 \Delta_{r\theta} U + L_0 U$ and $\tilde{F}(U_t, \mu) = [D(\mu + \nu^*) - D_0]\Delta_{r\theta} U + [L(\mu + \nu^*) - L_0]U_t + F(U_t, \mu)$. $D_0 = D(\nu^*)$, $L_0 = L(\nu^*)$ are obtained by the following Taylor expansions

$$D(\mu + \nu^*) = D_0 + \mu_1 D_1^{(1,0)} + \mu_2 D_1^{(0,1)} + \frac{1}{2}\left(\mu_1^2 D_2^{(2,0)} + 2\mu_1\mu_2 D_2^{(1,1)} + \mu_2^2 D_2^{(0,2)}\right) + \cdots,$$
$$L(\mu + \nu^*) = L_0 + \mu_1 L_1^{(1,0)} + \mu_2 L_1^{(0,1)} + \frac{1}{2}\left(\mu_1^2 L_2^{(2,0)} + 2\mu_1\mu_2 L_2^{(1,1)} + \mu_2^2 L_2^{(0,2)}\right) + \cdots.$$

We will conduct subsequent bifurcation analysis based on system (4).

III. MAIN RESULTS

A. Bifurcation analysis and normal forms

In this section, the center manifold reduction and normal form method are employed to simplify the bifurcation problem. Based on the Turing-Hopf normal forms theory for reaction-diffusion systems in a one-dimensional interval [29, 30], we will derive the normal forms for ET-H, T-EH, and ET-EH bifurcations on a disk, respectively. If (ET-EH) holds, both the Turing and Hopf

portions are affected by symmetry. At this time, the center subspace of the equilibrium is six-dimensional and the result is the most complex. Therefore, let's first tackle this difficult problem. Normal forms in polar coordinates are used to represent the changes in amplitude (ρ) and complex angle (χ) of the solutions under different oscillation modes, and the mathematical derivation is shown in the Appendix. When $n_{T_3} \neq 2n_{H_3}$ or $n_{T_3} = 2n_{H_3}$, there will be two different normal forms.

When $n_{T_3} \neq 2n_{H_3}$, the normal form truncated to the third order for the ET-EH bifurcation can be written in polar coordinates as

$$\begin{aligned}
\dot{\rho}_{H^1} &= (\varepsilon_1(\mu) + c_{11}\rho_{H^1}^2 + c_{12}\rho_{H^2}^2 + c_{13}\rho_{T^1}\rho_{T^2})\rho_{H^1}, \\
\dot{\rho}_{H^2} &= (\varepsilon_1(\mu) + c_{11}\rho_{H^2}^2 + c_{12}\rho_{H^1}^2 + c_{13}\rho_{T^1}\rho_{T^2})\rho_{H^2}, \\
\dot{\rho}_{T^1} &= (\varepsilon_2(\mu) + c_{21}\rho_{H^1}^2 + c_{22}\rho_{H^2}^2 + c_{23}\rho_{T^1}\rho_{T^2})\rho_{T^1}, \\
\dot{\rho}_{T^2} &= (\varepsilon_2(\mu) + c_{21}\rho_{H^1}^2 + c_{22}\rho_{H^2}^2 + c_{23}\rho_{T^1}\rho_{T^2})\rho_{T^2}.
\end{aligned} \tag{5}$$

This a four-dimensional real ordinary differential equations (ODEs) with ρ_{H^1}, ρ_{H^2}, ρ_{T^1} and ρ_{T^2} as independent variables, where $\rho_{H^i}, i = 1,2$ are variables on the eigenspace corresponding to pure imaginary roots $\pm \mathrm{i}\omega_{H_3}$ (Hopf) and $\rho_{T^i}, i = 1,2$ correspond to the zero root (Turing). When $n_{T_3} = 2n_{H_3}$, there will be additional terms like $z_3 z_5 e_1, z_4 z_5 e_2$, $z_1 z_6 e_3$and $z_2 z_6 e_4$ in the normal form. If we use the same polar coordinate transformation, a phase shift between two Hopf modes $\Delta\chi = \chi_{H^1} - \chi_{H^2}$ will appear as a new variable, i.e., the normal form written in polar coordinates becomes

$$\begin{aligned}
\dot{\rho}_H &= (\varepsilon_1(\mu) + (c_{11} + c_{12})\rho_H^2 + c_{13}\rho_T^2 + c_{14}\rho_T \cos\Delta\chi)\rho_H, \\
\dot{\Delta\chi} &= -2c_{14}\rho_T \sin\Delta\chi, \\
\dot{\rho}_T &= (\varepsilon_2(\mu) + (c_{21} + c_{22})\rho_H^2 + c_{23}\rho_T^2)\rho_T.
\end{aligned} \tag{6}$$

For $\Delta\chi = 0$ or π, two Fourier modes are in-phase or anti-phase.

The normal forms for ET-H and T-EH bifurcations can be considered as parts of the normal form of the ET-EH bifurcation, and the derivation is somewhat simpler. Therefore, based on the derivation provided in the Appendix, it is easy to obtain normal forms of ET-H and T-EH bifurcations, respectively. If (ET-H) holds, the dimension of the eigenspace corresponding to pure imaginary roots $\pm \mathrm{i}\omega_{H_2}$ decreases. By (18) and (19), we can obtain that the normal form truncated to the third order for ET-H bifurcation in polar coordinates is

$$\begin{aligned}
\dot{\rho}_H &= (\alpha_1(\mu) + a_{11}\rho_H^2 + a_{12}\rho_{T^1}\rho_{T^2})\rho_H, \\
\dot{\rho}_{T^1} &= (\alpha_2(\mu) + a_{21}\rho_{T^1}\rho_{T^2} + a_{22}\rho_H^2)\rho_{T^1},. \\
\dot{\rho}_{T^2} &= (\alpha_2(\mu) + a_{21}\rho_{T^1}\rho_{T^2} + a_{22}\rho_H^2)\rho_{T^2}.
\end{aligned} \tag{7}$$

If (T-EH) holds, the dimension of the eigenspace corresponding to the zero root decreases and the the normal form truncated to the third order for T-EH bifurcation in polar coordinates is

$$\begin{aligned}
\dot{\rho}_{H^1} &= (\beta_1(\mu) + b_1\rho_T + b_{11}\rho_{H^1}^2 + b_{12}\rho_{H^2}^2 + b_{13}\rho_T^2)\rho_{H^1}, \\
\dot{\rho}_{H^2} &= (\beta_1(\mu) + b_1\rho_T + b_{11}\rho_{H^2}^2 + b_{12}\rho_{H^1}^2 + b_{13}\rho_T^2)\rho_{H^2}, \\
\dot{\rho}_T &= (\beta_2(\mu) + b_2\rho_T + b_{21}\rho_{H^1}^2 + b_{22}\rho_{H^2}^2 + b_{23}\rho_T^2)\rho_T.
\end{aligned} \tag{8}$$

B. Classification of pattern solutions

The normal form on the center manifold inherits the dynamic properties of the original system, and equilibrium points of (5) to (8) correspond to different wave patterns. Therefore, we will follow this approach to classify the possible wave patterns induced by equivariant Turing-Hopf bifurcations in detail in this subsection.

1. ET-EH patterns

When $n_{T_3} \neq 2n_{H_3}$, we are mainly concerned with the properties corresponding to the following fourteen equilibrium points of (5), which are separated into five categories.

(ET-EH-i) ***Stationary solution***. $(\rho_{H^1}, \rho_{H^2}, \rho_{T^1}, \rho_{T^2}) = (0,0,0,0)$ corresponds to the origin in the six-dimensional phase space, which is spatially homogeneous.

(ET-EH-ii) ***Static Turing pattern***. $(\rho_{H^1}, \rho_{H^2}, \rho_{T^1}, \rho_{T^2}) = (0,0,\rho_{T^1}, \rho_{T^2})$ with $\rho_{T^1}\rho_{T^2} = -\varepsilon_2(\mu)/c_{23}$.

(ET-EH-iii) ***Rotating wave pattern***. In this case, for $\varepsilon_1(\mu)c_{11} < 0$, $(\rho_{H^1}, \rho_{H^2}, \rho_{T^1}, \rho_{T^2}) = (0, \sqrt{-\varepsilon_1(\mu)/c_{11}}, 0, 0)$ and $(\rho_{H^1}, \rho_{H^2}, \rho_{T^1}, \rho_{T^2}) = (\sqrt{-\varepsilon_1(\mu)/c_{11}}, 0, 0, 0)$ correspond to the periodic solutions in the subspace of (z_2, z_3) and (z_1, z_4), respectively. The periodic solutions restricted to the center subspace has one of the following approximate forms.

$$U(t)(r,\theta) \approx \sum_{i=1}^{n} 2|p_{1i}|\sqrt{\frac{-\varepsilon_1(\mu)}{c_{11}}} J_{n_{H_3}}(\sqrt{\lambda_{n_{H_3}m_{H_3}}}r)\cos(\mathrm{Arg}(p_{1i}) + \omega_{H_3}t \pm n_{H_3}\theta)\mathbf{e}_i,$$

where $\mathbf{e}_i$ is the ith unit coordinate vector of $\mathbb{R}^n$ and $p_{1i}, 1 \leq i \leq n$ are defined in the Appendix. The physical solutions in (ET-EH-iii) are spatially inhomogenous oscillations with frequency ω_{H_3} and rotates clockwise or anticlockwise, which can be inferred from the sign before $n_{H_3}\theta$.

(ET-EH-iv) ***Standing wave pattern***. In this case, $(\rho_{H^1}, \rho_{H^2}, \rho_{T^1}, \rho_{T^2}) = \left(\sqrt{\frac{-\varepsilon_1(\mu)}{c_{11}+c_{12}}}, \sqrt{\frac{-\varepsilon_1(\mu)}{c_{11}+c_{12}}}, 0, 0\right)$,

the periodic solution restricted to the center subspace has the following approximate form

$$U(t)(r,\theta)\approx\sum_{i=1}^{n}4|p_{1i}|\sqrt{\frac{-\varepsilon_1(\mu)}{c_{11}+c_{12}}}J_{n_{H_3}}(\sqrt{\lambda_{n_{H_3}m_{H_3}}}r)\cos(\mathrm{Arg}(p_{1i})+\omega_{H_3}t)\cos(n_{H_3}\theta)\mathbf{e}_i.$$

The physical solution in (ET-EH-iv) is also a spatially inhomogenous oscillation with frequency ω_{H_3}. However, the existence of a fixed axis is out of the ordinary, which can be obtained from $\cos(n_{H_3}\theta)=0$.

(ET-EH-v) ***Mixed ET-EH pattern***. In this case, there are nine groups of ET-EH patterns.

(a) $(\rho_{H^1},\rho_{H^2},\rho_{T^1},\rho_{T^2})=\left(0,\sqrt{\frac{c_{13}\varepsilon_2(\mu)-c_{23}\varepsilon_1(\mu)}{c_{23}c_{11}-c_{13}c_{22}}},\rho_{T^1},\rho_{T^2}\right)$ with $\rho_{T^1}\rho_{T^2}=-(\varepsilon_1(\mu)+c_{11}\rho_{H^2}^2)/c_{13}$, or $\left(0,\sqrt{\frac{-\varepsilon_1(\mu)}{c_{11}}},0,\rho_{T^2}\right)$ and $\left(0,\sqrt{\frac{-\varepsilon_1(\mu)}{c_{11}}},\rho_{T^1},0\right)$ with $\frac{\varepsilon_1(\mu)}{c_{11}}=\frac{\varepsilon_2(\mu)}{c_{22}}$, correspond to three groups of **type-A mixed ET-EH patterns**. At these points, the solution of real form restricted to the center subspace has the following approximate form

$$\begin{aligned}U(t)(r,\theta)\approx&\sum_{i=1}^{n}2|p_{1i}|\rho_{H^2}J_{n_{H_3}}(\sqrt{\lambda_{n_{H_3}m_{H_3}}}r)\cos(\mathrm{Arg}(p_{1i})+\omega_{H_3}t+n_{H_3}\theta)\mathbf{e}_i\\&+\xi_T\,(\rho_{T^1}+\rho_{T^2})\,J_{n_{T_3}}(\sqrt{\lambda_{n_{T_3}m_{T_3}}}r)\cos(n_{T_3}\theta).\end{aligned}\tag{9}$$

(b) $(\rho_{H^1},\rho_{H^2},\rho_{T^1},\rho_{T^2})=\left(\sqrt{\frac{c_{13}\varepsilon_2(\mu)-c_{23}\varepsilon_1(\mu)}{c_{23}c_{11}-c_{13}c_{21}}},0,\rho_{T^1},\rho_{T^2}\right)$ with $\rho_{T^1}\rho_{T^2}=-(\varepsilon_1(\mu)+c_{11}\rho_{H^1}^2)/c_{13}$, or $\left(\sqrt{\frac{-\varepsilon_1(\mu)}{c_{11}}},0,0,\rho_{T^2}\right)$ and $\left(\sqrt{\frac{-\varepsilon_1(\mu)}{c_{11}}},0,\rho_{T^1},0\right)$ with $\frac{\varepsilon_1(\mu)}{c_{11}}=\frac{\varepsilon_2(\mu)}{c_{22}}$, correspond to three groups of **type-B mixed ET-EH patterns**. At these points, the solution restricted to the center subspace has the following approximate form

$$\begin{aligned}U(t)(r,\theta)\approx&\sum_{i=1}^{n}2|p_{1i}|\rho_{H^1}J_{n_{H_3}}(\sqrt{\lambda_{n_{H_3}m_{H_3}}}r)\cos(\mathrm{Arg}(p_{1i})+\omega_{H_3}t-n_{H_3}\theta)\mathbf{e}_i\\&+\xi_T\,(\rho_{T^1}+\rho_{T^2})\,J_{n_{T_3}}(\sqrt{\lambda_{n_{T_3}m_{T_3}}}r)\cos(n_{T_3}\theta).\end{aligned}\tag{10}$$

(c) $(\rho_{H^1},\rho_{H^2},\rho_{T^1},\rho_{T^2})=\left(\sqrt{\frac{c_{13}\varepsilon_2(\mu)-c_{23}\varepsilon_1(\mu)}{c_{23}(c_{11}+c_{12})-c_{13}(c_{21}+c_{22})}},\sqrt{\frac{c_{13}\varepsilon_2(\mu)-c_{23}\varepsilon_1(\mu)}{c_{23}(c_{11}+c_{12})-c_{13}(c_{21}+c_{22})}},\rho_{T^1},\rho_{T^2}\right)$ with $\rho_{T^1}\rho_{T^2}=-\frac{\varepsilon_1(\mu)+(c_{11}+c_{12})\rho_{H^1}^2}{c_{13}}$, or $\left(\sqrt{\frac{-\varepsilon_1(\mu)}{c_{11}+c_{12}}},\sqrt{\frac{-\varepsilon_1(\mu)}{c_{11}+c_{12}}},\rho_{T^1},0\right)$ and $\left(\sqrt{\frac{-\varepsilon_1(\mu)}{c_{11}+c_{12}}},\sqrt{\frac{-\varepsilon_1(\mu)}{c_{11}+c_{12}}},0,\rho_{T^2}\right)$ with $\frac{\varepsilon_1(\mu)}{c_{11}+c_{12}}=\frac{\varepsilon_2(\mu)}{c_{21}+c_{22}}$ correspond to three groups of **type-C mixed ET-EH patterns**. At these point, the solution restricted to the center subspace has the following approximate form

$$\begin{aligned}U(t)(r,\theta)\approx&\sum_{i=1}^{n}4|p_{1i}|\rho_{H^1}J_{n_{H_3}}(\sqrt{\lambda_{n_{H_3}m_{H_3}}}r)\cos(\mathrm{Arg}(p_{1i})+\omega_{H_3}t)\cos(n_{H_3}\theta)\mathbf{e}_i\\&+\xi_T\,(\rho_{T^1}+\rho_{T^2})\,J_{n_{T_3}}(\sqrt{\lambda_{n_{T_3}m_{T_3}}}r)\cos(n_{T_3}\theta).\end{aligned}\tag{11}$$

We demonstrated the specific forms of rotating and standing wave patterns in our previous work [42]. Now, let's discuss the mixed ET-EH patterns. (ET-EH-v) shows three types of complex mixed ET-EH patterns. We draw a schematic diagram in Fig. 1 of the solution in (9) with $n_{T_3} = 1, m_{T_3} = 1$; $n_{H_3} = 2, m_{H_3} = 2$ and $\omega_{H_3} = 1$ as an example, which is

$$U(t)(r,\theta) \approx J_2(\sqrt{\lambda_{22}}r)\cos(t+2\theta) + J_1(\sqrt{\lambda_{11}}r)\cos\theta. \tag{12}$$

The subfigures in the first row provide mixed ET-EH patterns like (9) at $t = 0,\ T/3,\ 2T/3$, and T, respectively, where $T \approx 6$ is the period. Fixing $r = R$ and $r = R/2$, we find that despite (12) is a sum of two regular patterns generating from Hopf bifurcation and Turing instability, under the interaction of the two, the spatial form of (12) is quite complex, making it difficult to summarize general rule. Similarly, the solutions in (10) and (11) can be explained in the same way.

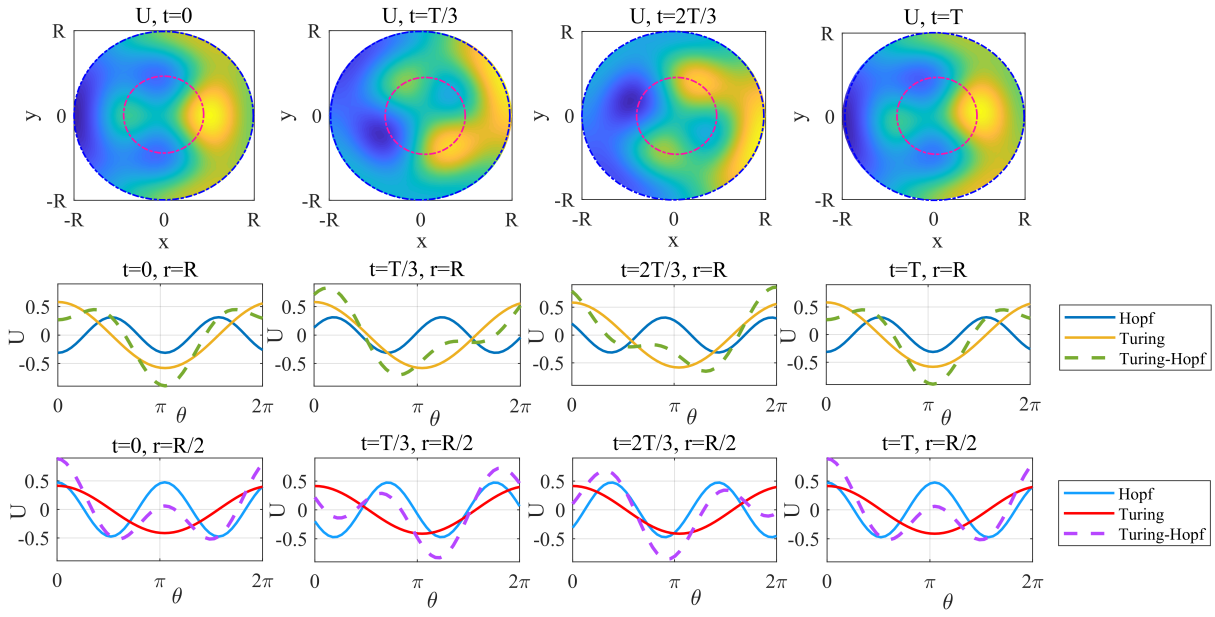

FIG. 1: First row: Mixed ET-EH patterns in (12). Second/Third row: At $r = R/r = \frac{R}{2}$, the Hopf component, Turing component and there sum of (12) are illustrated.

When $n_{T_3} = 2n_{H_3}$, we are more concerned about the form of the original system solution corresponds to the equilibrium point of (6) with $\rho_H \neq 0,\ \rho_T \neq 0$ and $\Delta\chi \neq 0$, for instance, $(\rho_H, \rho_T, \Delta\chi) = \left(\sqrt{\frac{c_{23}\rho_T^2+\varepsilon_2(\mu)}{c_{21}+c_{22}}},\ \frac{-C_2\pm\sqrt{C_2^2-4C_1C_3}}{2C_1}, \pi\right)$, with $C_1 = (c_{11}+c_{12})c_{23}+(c_{21}+c_{22})c_{13}$, $C_2 = \frac{-(c_{21}+c_{22})c_{14}\pi}{2}$, $C_3 = (c_{11}+c_{12})\varepsilon_2(\mu)+(c_{21}+c_{22})\varepsilon_1(\mu)$. At these points, the solution restricted to

the center subspace has the following approximate form

$$\begin{aligned} U(t)(r,\theta) \approx & -\sum_{i=1}^{n} 4|p_{1i}|\rho_H J_{n_{H_3}}(\sqrt{\lambda_{n_{H_3}m_{H_3}}}r)\sin(\mathrm{Arg}(p_{1i})+\chi_{H^1}(t))\sin(n_{H_3}\theta)\mathbf{e}_i \\ & +2\xi_T\rho_T J_{n_{T_3}}(\sqrt{\lambda_{n_{T_3}m_{T_3}}}r)\cos(n_{T_3}\theta). \end{aligned} \tag{13}$$

It can be observed that two Fourier modes of the equivariant Hopf parts are anti-phase, with a shift $\Delta\chi = \chi_{H^1} - \chi_{H^2} = \pi$, which ultimately manifests as π phase difference in the Hopf part and Turing part of the expression (13). Thus, the form of solution maintains standing wave characteristics (Hopf) and static pattern characteristics (Turing) at opposite positions on the disk.

2. ET-H patterns

We can explain dynamics of the system by analyzing five equilibrium points of system (7). The equilibrium points $(0,0,0)$ and $(0,\rho_{T^1},\rho_{T^2})$ with $\rho_{T^1}\rho_{T^2} = -\frac{\alpha_2(\mu)}{a_{21}}$ are similar to (ET-EH-i)-(ET-EH-ii), but the dynamic properties of the other equilibrium points are simpler than (ET-EH-v). Therefore, we only introduce the following mixed mode.

(ET-H-i) ***Breathing pattern***. $(\rho_H,\rho_{T^1},\rho_{T^2}) = \left(\sqrt{\frac{a_{12}\alpha_2(\mu)-a_{21}\alpha_1(\mu)}{a_{11}a_{21}-a_{12}a_{22}}},\rho_{T^1},\rho_{T^2}\right)$ with $\rho_{T^1}\rho_{T^2} = \frac{\alpha_1(\mu)+a_{11}\rho_H^2}{-a_{12}}$, or $(\sqrt{\frac{-\alpha_1(\mu)}{a_{11}}},\rho_{T^1},0)$ and $(\sqrt{\frac{-\alpha_1(\mu)}{a_{11}}},0,\rho_{T^1})$ with $\frac{\alpha_1(\mu)}{a_{11}} = \frac{\alpha_2(\mu)}{a_{22}}$, correspond to three groups of dynamic Turing-Hopf patterns. At these points, the solution restricted to the center subspace has the following approximate form

$$\begin{aligned} U(t)(r,\theta) \approx & \sum_{i=1}^{n} 2|p_{1i}|\rho_H J_0(\sqrt{\lambda_{p_{H_1}}}r)\cos(\mathrm{Arg}(p_{1i})+\omega_{H_1}t)\mathbf{e}_i \\ & +\xi_T(\rho_{T^1}+\rho_{T^2})J_{n_{T_1}}(\sqrt{\lambda_{n_{T_1}m_{T_1}}}r)\cos(n_{T_1}\theta). \end{aligned}$$

The physical solution will maintain a fixed inhomogeneous form and oscillate up and down over time with frequency ω_{H_1} (breathing).

Further research on stability of the solution can be conducted to achieve pattern control. Let $\rho_T^2 = \rho_{T^1}\rho_{T^2}$, $\bar{\rho}_H = \rho_H\sqrt{|a_{11}|}$, $\bar{\rho}_T = \rho_T\sqrt{|a_{21}|}$, and drop the bars, then system (7) can be transformed into

$$\begin{aligned} \dot{\rho}_H &= (\alpha_1(\mu)+\rho_H^2+a_b\rho_T^2)\rho_H, \\ \dot{\rho}_T &= (\alpha_2(\mu)+a_c\rho_H^2+a_d\rho_T^2)\rho_T, \end{aligned} \tag{14}$$

which has 12 distinct kinds of unfoldings. The stability conditions of equilibrium points can be given, by Chap. 7.5 in [54]. Thus, in this case, the stability of spatiotemporal solutions and a

complete bifurcation set are easily obtained and there will be a quasi-periodic solution on the three-dimensional torus.

(ET-H-ii) ***Quasi-periodic ET-H pattern***. Here, the solution corresponds to that system (14) has a center and level curves with $\rho_H^2 + \upsilon\rho_T^2 = -\alpha_1(\mu)$ where $\upsilon = \frac{a_b+1}{a_c-1}$. The solution generated by the Hopf bifurcation restricted to the center subspace has the following approximate form:

$$\begin{aligned} U(t)(r,\theta) \approx & \sum_{i=1}^{n} 2|p_{1i}|\rho_H J_0(\sqrt{\lambda_{p_{H_1}}}r)\cos(\mathrm{Arg}(p_{1i}) + \omega_{H_1}t)\cos(\bar{\omega}t)\mathbf{e}_i \\ & + \xi_T\rho_T J_{n_{T_1}}(\sqrt{\lambda_{n_{T_1}m_{T_1}}}r)\cos(n_{T_1}\theta)\sin(\bar{\omega}t), \end{aligned}$$

where $\bar{\omega} = O(\alpha_i(\mu))$. This is a rather complicated pattern including one spatial frequency and two different temporal frequencies, which is actually a quasi-periodic oscillation with spatial inhomogeneous profiles.

3. T-EH patterns

We can explain dynamics of the system by analyzing at most twelve equilibrium points of system (8). Similar to Sec. III B 2, several equilibrium points of system (8) are consistent with the results of ET-EH patterns. Next, we will explain in detail several solutions for the interaction of Turing-Hopf under (T-EH), which is more clearer than (ET-EH-v).

(T-EH-i) ***Rotating wave-like T-EH pattern***. In this case, $(\rho_{H^1}, \rho_{H^2}, \rho_T) = (0, \sqrt{\frac{\beta_1(\mu)+b_1\rho_T+b_{13}\rho_T^2}{-b_{11}}}, \frac{-B_2\pm\sqrt{B_2^2-4B_1B_3}}{2B_1})$ with $B_1 = b_1b_{22} - b_2b_{11},\ B_2 = b_{22}b_{13} - b_{11}b_{23},\ B_3 = b_{22}\beta_1(\mu) - b_{11}\beta_2(\mu)$, correspond to at most two periodic solutions, depending on the sign of $B_2^2 - 4B_1B_3$. Similarly, $(\rho_{H^1}, \rho_{H^2}, \rho_T) = \left(\sqrt{\frac{\beta_1(\mu)+b_1\rho_T+b_{13}\rho_T^2}{-b_{11}}}, 0, \frac{-B_5\pm\sqrt{B_5^2-4B_4B_6}}{2B_4}\right)$ with $B_4 = b_1b_{21} - b_2b_{11},\ B_5 = b_{21}b_{13} - b_{11}b_{23},\ B_6 = b_{21}\beta_1(\mu) - b_{11}\beta_2(\mu)$, correspond to at most another two periodic solutions. At these points, the periodic solution restricted to the center subspace has the following approximate forms

$$\begin{aligned} U(t)(r,\theta) \approx & \sum_{i=1}^{n} 2|p_{1i}|\rho_{H^2}J_{n_{H_2}}(\sqrt{\lambda_{n_{H_2}m_{H_2}}}r)\cos(\mathrm{Arg}(p_{1i}) + \omega_{H_2}t + n_{H_2}\theta)\mathbf{e}_i \\ & + \xi_T\rho_T J_0(\sqrt{\lambda_{p_{T_2}}}r), \end{aligned}$$

or

$$\begin{aligned} U(t)(r,\theta) \approx & \sum_{i=1}^{n} 2|p_{1i}|\rho_{H^2}J_{n_{H_2}}(\sqrt{\lambda_{n_{H_2}m_{H_2}}}r)\cos(\mathrm{Arg}(p_{1i}) + \omega_{H_2}t - n_{H_2}\theta)\mathbf{e}_i \\ & + \xi_T\rho_T J_0(\sqrt{\lambda_{p_{T_2}}}r). \end{aligned}$$

Similarly, the spatial form of the Turing component is constant. Therefore, along with a circle with radius r on the disk, the solution will be in the form of a clockwise or counterclockwise rotating wave.

(T-EH-ii) ***Standing wave-like T-EH pattern***. In this case, $(\rho_{H^1},\rho_{H^2},\rho_T)=(\sqrt{\frac{\beta_1(\mu)+b_1\rho_T+b_{13}\rho_T^2}{-(b_{11}+b_{12})}},\sqrt{\frac{\beta_1(\mu)+b_1\rho_T+b_{13}\rho_T^2}{-(b_{11}+b_{12})}},\frac{-B_8\pm\sqrt{B_8^2-4B_7B_9}}{2B_7})$ with $B_7=(b_{21}+b_{22})b_{13}-(b_{11}+b_{12})b_{23}$, $B_8=(b_{21}+b_{22})b_1-(b_{11}+b_{12})b_2$, $B_9=(b_{21}+b_{22})\beta_1(\mu)-(b_{11}+b_{12})\beta_2(\mu)$, correspond to at most two periodic solutions. At these points, the periodic solution restricted to the center subspace has the following approximate form

$$\begin{aligned}U(t)(r,\theta)\approx&\sum_{i=1}^{n}4|p_{1i}|\rho_{H^1}J_{n_{H_2}}(\sqrt{\lambda_{n_{H_2}m_{H_2}}}r)\cos(\mathrm{Arg}(p_{1i})+\omega_{H_2}t)\cos(n_{H_2}\theta)\mathbf{e}_i\\&+\xi_T\rho_T J_0(\sqrt{\lambda_{p_{T_2}}}r).\end{aligned}$$

IV. NUMERICAL SIMULATIONS AND APPLICATIONS

Avoiding critical points through spatial self-organization is very common in ecosystems, such as patterns formed by mussels and algae on tidal flats, which can avoid critical points caused by rising sea levels and protect tidal flats from being submerged [55, 56]. In [57], Shen and Wei investigated a delayed mussel-algae system and gave the dynamic classification near the Turing-Hopf bifurcation point in one-dimensional interval $(0,l\pi)$. Considering the local tidal flats in natural living environments or artificially cultivated mussels and freshwater algae in lakes, it is more realistic to establish mathematical models in circular domains. Therefore, we investigate the dynamics of such a model on a disk.

$$\begin{cases}\frac{\partial m(t,r,\theta)}{\partial t}=d_1\Delta_{r\theta}m(t,r,\theta)+m(t,r,\theta)\left[ba(t-\tau,r,\theta)-\frac{1}{1+m(t-\tau,r,\theta)}\right],\ (r,\theta)\in\mathbb{D},\ t>0,\\ \frac{\partial a(t,r,\theta)}{\partial t}=\Delta_{r\theta}a(t,r,\theta)+\alpha\left[1-a(t,r,\theta)\right]-m(t,r,\theta)a(t,r,\theta),\ (r,\theta)\in\mathbb{D},\ t>0,\\ \partial_r m(\cdot,R,\theta)=\partial_r a(\cdot,R,\theta)=0,\ \theta\in[0,2\pi).\end{cases}\tag{15}$$

For simplicity, we established a normalized model, where $m(t,r,\theta)$ and $a(t,r,\theta)$ represent the mussel biomass density and the algae concentration at location (r,θ) and time t, respectively. The mussel is on the sediment, and the algae live in the lower water layer overlying the mussel bed. b is related to the ingested algae-to-mussel biomass production, α is related to the rate of exchange between the lower and upper water layers, and τ is the digestion period of mussel. In the real world, limited sources, like nutrients and light, can lead to nonlocal intraspecific competition

among algae in the ocean [58, 59]. For the convenience of mathematical calculation, we take the nonlocal effects on the disk here. That is to say, based on system (15), we introduced nonlocal effects by replacing $\alpha(1-a(t,r,\theta))$ by $\alpha(1-\hat{a}(t,r,\theta))$ with

$$\hat{a}(t,r,\theta)=\frac{1}{\pi R^2}\int_0^R\int_0^{2\pi}\bar{r}a\left(t,\bar{r},\bar{\theta}\right)\mathrm{d}\bar{\theta}\mathrm{d}\bar{r}.$$

Then, system (15) becomes

$$\begin{cases}\frac{\partial m(t,r,\theta)}{\partial t}=d_1\Delta_{r\theta}m(t,r,\theta)+m(t,r,\theta)\left[ba(t-\tau,r,\theta)-\frac{1}{1+m(t-\tau,r,\theta)}\right],\ (r,\theta)\in\mathbb{D},\ t>0,\\ \frac{\partial a(t,r,\theta)}{\partial t}=\Delta_{r\theta}a(t,r,\theta)+\alpha\left[1-\hat{a}(t,r,\theta)\right]-m(t,r,\theta)a(t,r,\theta),\ (r,\theta)\in\mathbb{D},\ t>0,\\ \partial_r m(\cdot,R,\theta)=\partial_r a(\cdot,R,\theta)=0,\ \theta\in[0,2\pi).\end{cases}\tag{16}$$

Fixing $b=1.5,\ \alpha=0.3,\ R=6$, we obtain partial bifurcation curves on the $d_1-\tau$ plane of system (15) and system (16) shown in Fig. 2, respectively. For system (15), we select $(d_1,\tau)=(0.042,6)$ and get a type of breathing patterns (see Fig. 3). For system (16), we select $(d_1,\tau)=(0.036,2.7)$, and get two different types of dynamic Turing-Hopf patterns. Similar to the results in [42], Turing-Hopf pattern is standing wave-like with a specific initial value (see Fig. 4), and with other initial values, rotating wave-like Turing-Hopf patterns appear (see Fig. 5).

The standing wave-like pattern has a fixed axis (see the subgraph corresponding to $y=0$ in Fig. 4) and a hot/cold spot indicating local maximum/minimum that does not change position over time (see the area on the right side of the fixed axis). The other parts of the pattern oscillate in the form of standing waves on both sides of the fixed axis (as shown in the subgraph corresponding to $x=0$ in Fig. 4). The rotating wave-like pattern in Fig. 5 has a portion of the pattern that remains unchanged in position and the other parts of the pattern that change in the form of rotating wave.

The pattern formed in the mussel-algae system is actually an external manifestation of mussel aggregation, and its main function is to increase population defense, including shedding caused by wave impacts and threats from predators [60, 61]. The study of the interaction between Turing instability, Hopf bifurcation, and symmetry reveals the formation mechanism of these new patterns, which helps to explore the changes in mussel biomass and two-dimensional spatial distribution, fully developing the mussel economy, and playing an ecological role in alleviating eutrophication in marine systems [62, 63].

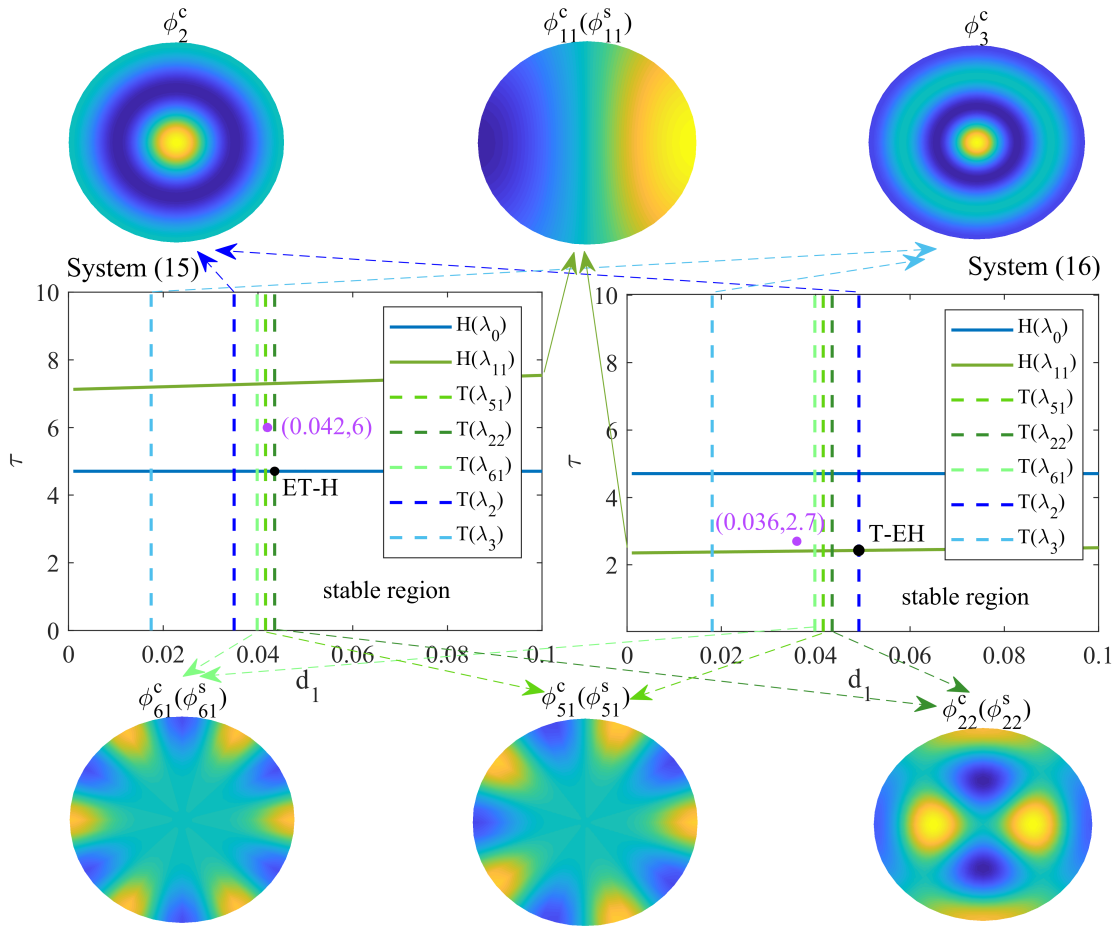

FIG. 2: Partial bifurcation curves on the $d_1-\tau$ plane for two systems and eigenfuncitons related to Turing instability.

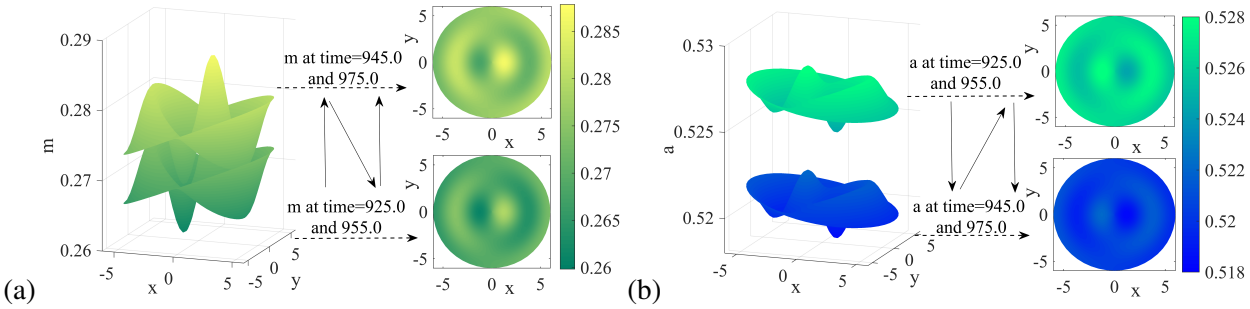

FIG. 3: System (15) produces breathing patterns with parameters:
$b=1.5,\ \alpha=0.3,\ R=6,\ d_1=0.042,\ \tau=6$. Initial values are $m(t,r,\theta)=0.2727+0.01\cdot\cos t\cdot\cos r\cdot\cos\theta,\ a(t,r,\theta)=0.5238+0.01\cdot\cos t\cdot\cos r\cdot\cos\theta,\ t\in[-\tau,0)$.
(a) : *The mussel*. (b) : *The algae*.

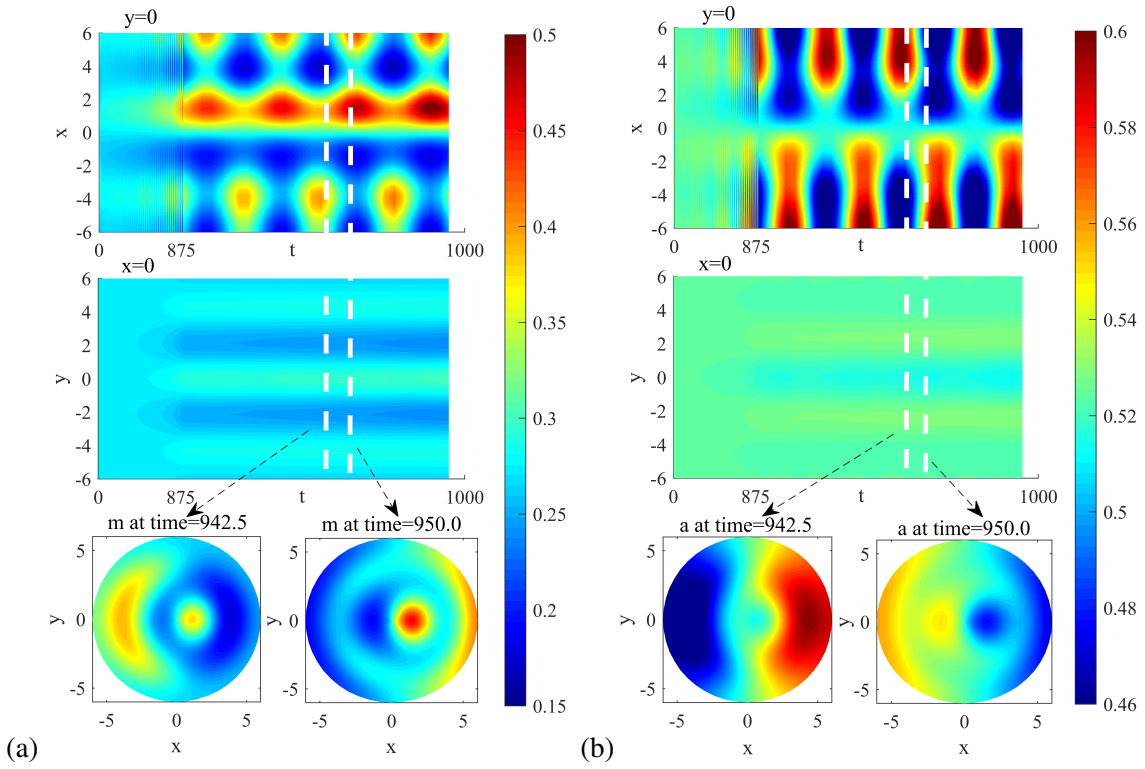

FIG. 4: System (16) produces standing wave-like T-EH patterns with parameters:
$b = 1.5,\ \alpha = 0.3,\ R = 6,\ d_1 = 0.036,\ \tau = 2.7$. Initial values are $m(t,r,\theta) = 0.2727 + 0.01 \cdot \cos t \cdot \cos r \cdot \cos\theta,\ a(t,r,\theta) = 0.5238 + 0.01 \cdot \cos t \cdot \cos r \cdot \cos\theta,\ t \in [-\tau, 0)$.
$(a) : The\ mussel.\ (b) : The\ algae.$

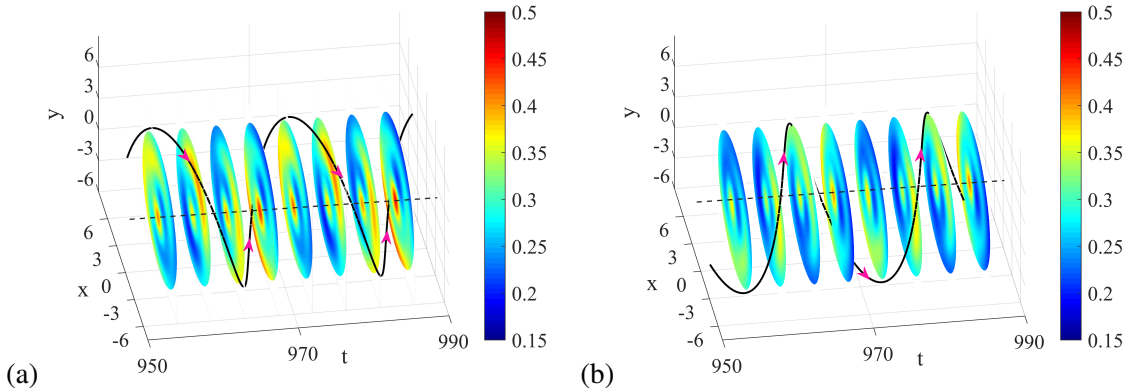

FIG. 5: Rotating wave-like T-EH patterns of the mussel with parameters:
$b = 1.5,\ \alpha = 0.3,\ R = 6,\ d_1 = 0.036,\ \tau = 2.7$. Initial values are $m(t,r,\theta) = 0.2727 + 0.01 \cdot \cos t \cdot \cos r \cdot \Theta_1(\theta),\ a(t,r,\theta) = 0.5238 + 0.01 \cdot \cos t \cdot \cos r \cdot \Theta_2(\theta),\ t \in [-\tau, 0)$.
$(a) : (\Theta_1(\theta), \Theta_2(\theta)) = (\cos\theta, \sin\theta) - clockwise,\ (b) : (\Theta_1(\theta), \Theta_2(\theta)) = (\sin\theta, \cos\theta) - anticlockwise.$

V. CONCLUDING REMARKS

In this paper, we investigate the interaction of Turing instability and Hopf bifurcation on a disk. We first present three Turing-Hopf normal forms based on different types of eigenspaces and then analyze the possible solutions for each normal form. Finally, breathing, standing wave-like, and rotating wave-like patterns were simulated in a specific mussel-algae model. In realistic models of approximate circular domains, patterns are often complex. The simple superposition of Turing instability and Hopf bifurcation is not enough to describe the temporal and spatial variations adequately. In this paper, our analysis of equivariant Turing-Hopf bifurcation and classification of various patterns can provide theoretical guidance for characterizing complex patterns in circular domains and finding realistic solutions with physical significance.

Under the case (ET-EH), the possible solutions are complex, and there are several questions that can be further discussed. We believe that quasi-periodic solutions may also exist, which is quite difficult to study. In addition, in previous studies on double Hopf bifurcation, the resonance may occur: if the ratio of two imaginary roots $\mathrm{i}\omega_1$ and $\mathrm{i}\omega_2$ is rational, some additional terms cannot be eliminated. In this paper, another kind of resonance of Turing and Hopf appears, i.e. $n_{T_3} = 2n_{H_3}$. Combining these factors and investigating the corresponding normal forms is a noteworthy issue to be further considered.

ACKNOWLEDGMENT

The authors would like to express great appreciation to the anonymous referees for their constructive comments on the manuscript.

APPENDIX: CALCULATION OF NORMAL FORMS

In this Appendix, we provide the decomposition of the phase space and the derivation of normal forms, by applying the method in [29–31], which leads to the results in Sec. III A.

Let $\Lambda_1 = \{\gamma : \Gamma_p(\gamma) = 0,\ \mathrm{Re}\gamma = 0\}$, $\Lambda_2 = \{\gamma : \Gamma_{nm}(\gamma) = 0,\ \mathrm{Re}\gamma = 0\}$. Define a bilinear pairing

$$(\psi, \varphi) = \int_0^R \int_0^{2\pi} r \left[\overline{\psi(0)}\varphi(0) - \int_{-\tau}^0 \int_{\xi=0}^{\vartheta} \overline{\psi(\xi - \vartheta)} \mathrm{d}\eta(\nu^*, \vartheta)\varphi(\xi)\mathrm{d}\xi \right] \mathrm{d}r\mathrm{d}\theta,\ \psi \in (\mathscr{C}^*)^n,\ \varphi \in \mathscr{C}^n, \tag{17}$$

where $(\mathscr{C}^*)^n$ is the dual space of $\mathscr{C}^n$. By [51, 52], one can decompose $C^n := C([-1,0],\mathbb{C}^n)$ by Λ_i as $C^n = P_i \oplus Q_i,\ i = 1,2$, where P_i is the generalised eigenspace associated with Λ_i and $Q_i = \{\phi \in \mathscr{C} :\ (\psi,\phi) = 0,\ for\ all\ \psi \in P_i^*\}$. Here, P_i^* is the dual space of P_i. Suitably, choose the bases $\Phi^i_{r\theta}$ and $\Psi^i_{r\theta}$ of P_i and P_i^*, respectively, such that $\left(\Psi^i_{r\theta},\Phi^i_{r\theta}\right) = I_{n_i}$, where $n_i = \dim P_i$. Analogously, the phase space $\mathscr{C}^n$ can be decomposed as $\mathscr{C}^n = \mathscr{P} \oplus \mathscr{Q}$, where $\mathscr{P} = \mathrm{Im}\pi,\ \mathscr{Q} = \mathrm{Ker}\pi,\ \dim\mathscr{P} = \sum_{i=1}^2 n_i$, and $\pi :\ \mathscr{X} \to \mathscr{P}$ is a projection defined by $\pi(U_t) = \sum_{i=1}^2 \left(\Phi^i_{r\theta}\langle\Psi^i_{r\theta},U_t\rangle\right)^{\mathrm{T}}$.

In Table I, we list roots with zero real part of the characteristic equation. For the case (ET-EH), we get that $\Lambda_1 = \emptyset,\ \Lambda_2 = \{\pm \mathrm{i}\omega_{H_3}, 0\}$. Let

$$\begin{aligned}
\Phi^2_{r\theta} =& \left(\Phi^{2(1)}\cdot\hat{\phi}^c_{nm_2},\ \Phi^{2(2)}\cdot\hat{\phi}^c_{nm_2},\ \Phi^{2(3)}\cdot\hat{\phi}^s_{nm_2},\ \Phi^{2(4)}\cdot\hat{\phi}^s_{nm_2},\ \Phi^{2(5)}\cdot\hat{\phi}^c_{nm_2},\ \Phi^{2(6)}\cdot\hat{\phi}^s_{nm_2}\right),\\
\Psi^2_{r\theta} =& \mathrm{col}\left(\Psi^{2(1)}\cdot\hat{\phi}^c_{nm_2},\ \Psi^{2(2)}\cdot\hat{\phi}^c_{nm_2},\ \Psi^{2(3)}\cdot\hat{\phi}^s_{nm_2},\ \Psi^{2(4)}\cdot\hat{\phi}^s_{nm_2},\ \Psi^{2(5)}\cdot\hat{\phi}^c_{nm_2},\ \Psi^{2(6)}\cdot\hat{\phi}^s_{nm_2}\right),
\end{aligned}$$

where $\Phi^{2(1)}(\vartheta) = \xi_H \mathrm{e}^{\mathrm{i}\omega_{H_3}\vartheta},\ \Phi^{2(2)}(\vartheta) = \overline{\Phi^{2(1)}(\vartheta)},\ \Phi^{2(3)}(\vartheta) = \Phi^{2(1)}(\vartheta),\ \Phi^{2(4)}(\vartheta) = \Phi^{2(2)}(\vartheta),\ \Phi^{2(5)} = \Phi^{2(6)} = \xi_T,\ \Psi^{2(1)}(\rho) = \eta_H^{\mathrm{T}}\mathrm{e}^{\mathrm{i}\omega_{H_3}\rho},\ \Psi^{2(2)}(\rho) = \overline{\Psi^{2(1)}(\rho)},\ \Psi^{2(3)}(\rho) = \Psi^{2(1)}(\rho),\ \Psi^{2(4)}(\rho) = \Psi^{2(2)}(\rho),\ \Psi^{2(5)} = \Psi^{2(6)} = \eta_T^{\mathrm{T}},\ n = n_{H_3},\ m = m_{H_3},\ \vartheta \in [-1,0),\ \rho \in (0,1]$. $\xi_H = (p_{11},p_{12},\cdots,p_{1n})^{\mathrm{T}} \in \mathbb{C}^n$ is the eigenvector associated with the eigenvalue $\mathrm{i}\omega$ and $\xi_T = (q_{11},q_{12},\cdots,q_{1n})^{\mathrm{T}} \in \mathbb{R}^n$ is the eigenvector associated with the eigenvalue 0. $\eta_H \in \mathbb{C}^n$ and $\eta_T \in \mathbb{R}^n$ are the corresponding adjoint eigenvectors that satisfy $\left(\Psi^2_{r\theta},\Phi^2_{r\theta}\right) = I_6$.

According to the definition of the projection π, $U_t = (u_{1t},u_{2t},\cdots,u_{nt})$ can be decomposed as $U_t = \left(\Phi^1_{r\theta}\langle\Psi^1_{r\theta},U_t\rangle\right)^{\mathrm{T}} + \left(\Phi^2_{r\theta}\langle\Psi^2_{r\theta},U_t\rangle\right)^{\mathrm{T}} + w_t = \Phi_{r\theta}z + w_t$, with $\Phi_{r\theta} = \Phi^2_{r\theta}$, $z = (z_1,z_2,z_3,z_4,z_5,z_6)^{\mathrm{T}}$, and $w_t \in \mathscr{Q}$. Notice that the part $\Phi^2_{r\theta}(z_1,z_2,z_3,z_4,z_5,z_6)^{\mathrm{T}}$ stands for the solution on the center manifold, by which solutions on the center manifold are approximatively given.

It is easy to verify that

$$\begin{aligned}
M^1_j(\mu^l z^p e_k) &:= D_z(z^p\mu^l e_k)Bz - Bz^p\mu^l e_k = \mathrm{i}\omega_{H_3}\left(p_1 - p_2 + p_3 - p_4 + (-1)^k\right)z^p\mu^l e_k,\ k = 1,2,3,4\\
M^1_j(\mu^l z^p e_k) &:= D_z(z^p\mu^l e_k)Bz - Bz^p\mu^l e_k = \mathrm{i}\omega_{H_3}\left(p_1 - p_2 + p_3 - p_4\right)z^p\mu^l e_k,\ k = 5,6,
\end{aligned} \tag{18}$$

with M^1_j defined in [31], $B = \mathrm{diag}\{\mathrm{i}\omega_{H_3},-\mathrm{i}\omega_{H_3},\mathrm{i}\omega_{H_3},-\mathrm{i}\omega_{H_3},0,0\}$, $j \geq 2$, $z^p = z_1^{p_1}z_2^{p_2}z_3^{p_3}z_4^{p_4}z_5^{p_5}z_6^{p_6}$, $\mu^l = \mu_1^{l_1}\mu_2^{l_2}$, $p_1+p_2+p_3+p_4+l_1+l_2 = j$, and $\{e_1,e_2,e_3,e_4,e_5,e_6\}$ being the canonical basis for $\mathscr{C}^6$. Therefore, after calculating two complementary space $\mathrm{Im}(M^1_2)^{\mathrm{c}}$ and $\mathrm{Im}(M^1_3)^{\mathrm{c}}$ like being done in [29, 42], the normal forms for Turing-Hopf bifurcation has the following form:

$$\dot{z} = Bz + \frac{1}{2!}g^1_2(z,0,\mu) + \frac{1}{3!}g^1_3(z,0,0) + o(|z||\mu|^2). \tag{19}$$

where $g_2^1(z,0,\mu)$ and $g_3^1(z,0,0)$ are composed of the projection on $\mathrm{Im}(M_2^1)^{\mathrm{c}}$ or $\mathrm{Im}(M_3^1)^{\mathrm{c}}$, which are defined in [31]. By the analysis in [29, 31, 42], noticing the fact

$$\int_0^R\int_0^{2\pi} r\left(\hat{\phi}^c_{n_{H_3}m_{H_3}}\right)^{k_1}\left(\hat{\phi}^s_{n_{H_3}m_{H_3}}\right)^{k_2}\left(\hat{\phi}^c_{n_{T_3}m_{T_3}}\right)^{k_3}\left(\hat{\phi}^s_{n_{T_3}m_{T_3}}\right)^{k_4}\mathrm{d}\theta\mathrm{d}r\begin{cases}\neq 0, & k_1n_{H_3}-k_2n_{H_3}+k_3n_{T_3}-k_4n_{T_3}=0,\\ =0, & others,\end{cases}$$

and the relationship of $\Phi_{r\theta}$ and $\Psi_{r\theta}$, we obtain that when $n_{T_3}\neq 2n_{H_3}$, the normal forms truncated to the third order for ET-EH bifurcation can be summarized as

$$\begin{aligned}
\dot{z}_1 =&\mathrm{i}\omega_{H_3}z_1+B_{11}\mu_1z_1+B_{21}\mu_2z_1+B_{100020}z_1z_5^2+B_{001020}z_3z_5^2+B_{100002}z_1z_6^2+B_{001002}z_3z_6^2\\
&+B_{210000}z_1^2z_2+B_{200100}z_1^2z_4+B_{012000}z_3^2z_2+B_{002100}z_3^2z_4+B_{111000}z_1z_2z_3+B_{101100}z_1z_3z_4\\
&+B_{100011}z_1z_5z_6+B_{001011}z_3z_5z_6,\\
\dot{z}_2 =&-\mathrm{i}\omega_{H_3}z_2+\overline{B_{11}}\mu_1z_2+\overline{B_{21}}\mu_2z_2+\overline{B_{100020}}z_2z_6^2+\overline{B_{001020}}z_4z_6^2+\overline{B_{100002}}z_2z_5^2+\overline{B_{001002}}z_4z_5^2\\
&+\overline{B_{210000}}z_1z_2^2+\overline{B_{200100}}z_2^2z_3+\overline{B_{012000}}z_4^2z_1+\overline{B_{002100}}z_4^2z_3+\overline{B_{111000}}z_1z_2z_4+\overline{B_{101100}}z_2z_3z_4,\\
&+\overline{B_{100011}}z_2z_5z_6+\overline{B_{001011}}z_2z_5z_6,\\
\dot{z}_5 =&B_{15}\mu_1z_5+B_{25}\mu_2z_5+B_{110010}z_1z_2z_5+B_{100110}z_1z_4z_5+B_{011010}z_2z_3z_5+B_{001110}z_3z_4z_5\\
&+B_{110001}z_1z_2z_6+B_{100101}z_1z_4z_6+B_{011001}z_2z_3z_6+B_{001101}z_3z_4z_6\\
&+B_{000030}z_5^3+B_{000003}z_6^3+B_{000021}z_5^2z_6+B_{000012}z_5z_6^2,
\end{aligned}\tag{20}$$

and the equations for z_3,z_4,z_6 are given by $z_1\leftrightarrow z_3$, $z_2\leftrightarrow z_4$ and $z_5\leftrightarrow z_6$ in the previous three equations. By [40], after a sequence of local invertible transformations, the normal form truncated to the third order can be reduced to

$$\begin{aligned}
\dot{z}_1 &= \mathrm{i}\omega_{H_3}z_1+B_{11}\mu_1z_1+B_{21}\mu_2z_1+B_{200100}z_1^2z_4+B_{111000}z_1z_2z_3+B_{100011}z_1z_5z_6,\\
\dot{z}_2 &= -\mathrm{i}\omega_{H_3}z_2+\overline{B_{11}}\mu_1z_2+\overline{B_{21}}\mu_2z_2+\overline{B_{200100}}z_3z_2^2+\overline{B_{111000}}z_1z_2z_4+\overline{B_{100011}}z_2z_5z_6,\\
\dot{z}_5 &= B_{15}\mu_1z_5+B_{25}\mu_2z_5+B_{100110}z_1z_4z_5+B_{011010}z_2z_3z_5+B_{000021}z_5^2z_6.
\end{aligned}\tag{21}$$

Again, the equations for z_3,z_4,z_6 are given by $z_1\leftrightarrow z_3$, $z_2\leftrightarrow z_4$ and $z_5\leftrightarrow z_6$. The proof is similar to Lemma III.2 of [42].

Through the change of variables $z_1=\rho_{H^1}\mathrm{e}^{\mathrm{i}\chi_{H^1}}$, $z_4=\rho_{H^1}\mathrm{e}^{-\mathrm{i}\chi_{H^1}}$, $z_3=\rho_{H^2}\mathrm{e}^{\mathrm{i}\chi_{H^2}}$, $z_2=\rho_{H^2}\mathrm{e}^{-\mathrm{i}\chi_{H^2}}$, $z_5=\rho_{T^1}$, $z_6=\rho_{T^2}$, we obtain (5) with $\varepsilon_1(\mu)=\mathrm{Re}\{B_{11}\}\mu_1+\mathrm{Re}\{B_{21}\}\mu_2$, $\varepsilon_2(\mu)=B_{15}\mu_1+B_{25}\mu_2$, $c_{11}=$

$\mathrm{Re}\{B_{200100}\}$, $c_{12} = \mathrm{Re}\{B_{111000}\}$, $c_{13} = \mathrm{Re}\{B_{100011}\}$, $c_{21} = B_{100110}$, $c_{22} = B_{011010}$, $c_{23} = B_{000021}$.

---

[1] W. Lampert and U. Sommer, *Limnoecology: The Ecology of Lakes and Streams* (Oxford University Press, New York, 2007).

[2] R. L. Baskin, G. Della Porta, and V. P. Wright, Dep. Rec. **8**, 39 (2022).

[3] M. Sheintuch and O. Nekhamkina, J. Chem. Phys. **107**, 8165 (1997).

[4] O. Nekhamkina and M. Sheintuch, Phys. A **249**, 134 (1998).

[5] A. V. Razgulin and T. E. Romanenko, Comput. Math. Math. Phys. **53**, 1626 (2013).

[6] T. E. Romanenko, Differ. Equ. **50**, 264 (2014).

[7] K. Chakraborty and V. Manthena, Nonlinear Dyn. **81**, 1895 (2015).

[8] Y. Lu, M. Xiao, J. Liang, J. Ding, Y. Zhou, Y. Wan, and C. Fan, IEEE Access **9**, 111326 (2021).

[9] J. M. Davidenko, A. V. Pertsov, R. Salomonsz, W. Baxter, and J. Jalife, Nature **355**, 349 (1992).

[10] F. X. Witkowski, L. J. Leon, P. A. Penkoske, W. R. Giles, M. L. Spano, W. L. Ditto, and A. T. Winfree, Nature **392**, 78 (1998).

[11] W. Lu, D. Yu, and R. G. Harrison, Phys. Rev. Lett. **76**, 3316 (1996).

[12] X. Zhang and K. Shen, Phys. Rev. E **63**, 046212 (2001).

[13] M. C. Cross and P. C. Hohenberg, Rev. Modern Phys. **65**, 851 (1993).

[14] A. M. Turing, Philos. Trans. R. Soc. Lond. Ser. A Math. Phys. Eng. Sci. **237**, 37 (1952).

[15] H. Poincaré, *Les méthodes nouvelles de la mécanique céleste, Vol. 1* (Gauthier-Villars, Paris, 1892).

[16] A. A. Andronov, C. R. Math. Acad. Sci. Paris **189**, 559 (1929).

[17] E. Hopf, Berichen Math. Phys. Kl. Säch. Akad. Wiss. Leipzig **94**, 1 (1942).

[18] J. J. Perraud, A. De Wit, E. Dulos, P. De Kepper, G. Dewel, and P. Borckmans, Phys. Rev. Lett. **71**, 1272 (1993).

[19] G. Heidemann, M. Bode, and H. G. Purwins, Phys. Lett. A **177**, 225 (1993).

[20] D. P. Vallette, W. S. Edwards, and J. P. Gollub, Phys. Rev. E **49**, R4783 (1994).

[21] X. Cao and W. Jiang, Nonlinear Anal. Real World Appl. **43**, 428 (2018).

[22] A. Rovinsky and M. Menzinger, Phys. Rev. A **46**, 6315 (1992).

[23] M. Meixner, A. De Wit, S. Bose, and E. Schöll, Phys. Rev. E **55**, 6690 (1997).

[24] S. Bose, P. Rodin, and E. Schöll, Phys. Rev. E **62**, 1778 (2000).

[25] W. Just, M. Bose, S. Bose, H. Engel, and E. Schöll, Phys. Rev. E **64**, 026219 (2001).

[26] M. Baurmann, T. Gross, and U. Feudel, J. Theoret. Biol. **245**, 220 (2007).

[27] N. A. Venkov, S. Coombes, and P. C. Matthews, Phys. D **232**, 1 (2007).

[28] A. Ledesma-Durán and J. L. Aragón, Commun. Nonlinear Sci. Numer. Simul. **83**, 105145 (2020).

[29] Y. Song, T. Zhang, and Y. Peng, Commun. Nonlinear Sci. Numer. Simul. **33**, 229 (2016).

[30] W. Jiang, Q. An, and J. Shi, J. Differential Equations **268**, 6067 (2020).

[31] T. Faria, Trans. Amer. Math. Soc. **352**, 2217 (2000).

[32] B. I. Camara, M. Haque, and H. Mokrani, Phys. A **461**, 374 (2016).

[33] R. Yang and Y. Song, Nonlinear Anal. Real World Appl. **31**, 356 (2016).

[34] N. Kumari and N. Mohan, Nonlinear Dyn. **100**, 763 (2020).

[35] P. Kumar and G. Gangopadhyay, Phys. Rev. E **101**, 042204 (2020).

[36] D. Wu and H. Zhao, J. Nonlinear Sci. **30**, 1015 (2020).

[37] Y. Lv, Nonlinear Dyn. **107**, 1357 (2021).

[38] M. Golubitsky, I. Stewart, and D. G. Schaeffer, *Singularities and Groups in Bifurcation Theory: Volume II* (Springer-Verlag, New York, 1989).

[39] S. Guo and J. Wu, *Bifurcation Theory of Functional Differential Equations* (Springer-Verlag, New York, 2013).

[40] S. A. van Gils and J. Mallet-Paret, Proc. Roy. Soc. Edinburgh Sect. A **104**, 279 (1986).

[41] S. Guo, J. Differential Equations **317**, 387 (2022).

[42] Y. Chen, X. Zeng, and B. Niu, "Equivariant Hopf bifurcation in a class of partial functional differential equations on a circular domain," (2023), arXiv:2305.05979 [math.DS].

[43] N. F. Britton, *Reaction-Diffusion Equations and Their Applications to Biology* (Academic Press, London, 1986).

[44] J. D. Murray, *Mathematical Biology: Spatial Models and Biomedical Applications* (Springer-Verlag, New York, 2003).

[45] Y. Song and X. Zou, Comput. Math. Appl. **67**, 1978 (2014).

[46] Q. An and W. Jiang, Int. J. Bifurcation Chaos **28**, 1850108 (2018).

[47] J. V. Noble, Nature **250**, 726 (1974).

[48] F. Li and X. Zhao, Bull. Math. Biol. **83**, 43 (2021).

[49] I. Lengyel and I. R. Epstein, Science **251**, 650 (1991).

[50] I. Lengyel and I. R. Epstein, Proc. Natl. Acad. Sci. USA **89**, 3977 (1992).

[51] J. K. Hale, *Theory of Functional Differential Equations* (Springer-Verlag, New York, 1977).

[52] J. Wu, *Theory and Applications of Partial Functional Differential Equations* (Springer-Verlag, New York, 1996).

[53] Y. Pinchover and J. Rubinstein, *An Introduction to Partial Differential Equations* (Cambridge University Press, 2005).

[54] J. Guckenheimer and P. Holmes, *Nonlinear Oscillations, Dynamical Systems, and Bifurcations of Vector Fields* (Springer-Verlag, New York, 1983).

[55] J. van de Koppel, J. C. Gascoigne, G. Theraulaz, M. Rietkerk, W. M. Mooij, and P. M. Herman, Science **322**, 739 (2008).

[56] Q.-X. Liu, P. M. Herman, W. M. Mooij, J. Huisman, M. Scheffer, H. Olff, and J. van De Koppel, Nat. Commun. **5**, 5234 (2014).

[57] Z. Shen and J. Wei, Int. J. Bifurcation Chaos **29**, 1950144 (2019).

[58] H. Steen, Bot. Mar. **46**, 36 (2003).

[59] K. M. Manoylov, J. Freshwater Ecol. **24**, 145 (2009).

[60] H. L. Hunt and R. E. Scheibling, Ecology **82**, 3213 (2001).

[61] H. L. Hunt and R. E. Scheibling, Veliger **45**, 273 (2002).

[62] J. Stadmark and D. J. Conley, Mar. Pollut. Bull. **62**, 1385 (2011).

[63] D. Rosioru, V. Abaza, C. Dumitrache, A. Filimon, and F. Timofte, in *14th International Multidisciplinary Scientific Geoconference Sgem 2014* (2014) pp. 569–576.